AIAA JOURNAL
Vol. 46, No. 3, March 2008

Active Control of Nonlinear Panel Flutter Using Aeroelastic Modes and Piezoelectric Actuators

Myounghee Kim,* Qinqin Li,† Jen-Kuang Huang,‡ and Chuh Mei§
Old Dominion University, Norfolk, Virginia 23508

DOI: 10.2514/1.33803

Suppression of nonlinear panel flutter at supersonic speeds has been investigated traditionally with system equations of motion in terms of in vacuo modal coordinates. For isotropic and symmetrically laminated orthotropic composite plates, the limit–cycle oscillations converged with six in vacuo natural modes at a zero yaw angle. However, as laminated composite plates undergo the effect of an arbitrary yawed flow angle, complicated characteristics emerge by increasing the required in vacuo natural modes for an analysis of limit–cycle oscillations. To design an effective controller, the large number of modes should be reduced. As a result, the small number of modes produces a capability to alleviate the costly computational effort in designing controllers for the suppression of nonlinear panel flutter. In the present study, aeroelastic modes that provide the reduced order basis are used for panel limit–cycle motion. Two or six to seven aeroelastic modes are implemented for developing an active controller of panel flutter with isotropic and anisotropic laminated composite plates at a zero or nonzero yaw angle. Along with the aeroelastic modal equations of lesser number, a linear quadratic regulator, which is one of the output feedback controllers, is constructed to suppress nonlinear panel flutter. An added extended Kalman filter compensates for the nonlinearity of structural motion resulting from updating the system information online. The norms of feedback control gain and the norms of Kalman filter estimation gain are employed for the optimal placement of PZT5A or macro-fiber composite piezoelectric actuators and sensors. Numerical results show that the designed controller based on aeroelastic modal coordinates can suppress the large-amplitude panel nonlinear flutter response. The maximum flutter-free dynamic pressure for isotropic and composite plates is evaluated to measure how much the performance is improved.

Nomenclature

$\bar{\mathbf{A}}$, $\mathbf{B}$, $\mathbf{C}$, $\mathbf{D}$	=	system state-space matrices
$[A]$, $[B]$, $[D]$	=	laminate extension, coupling, and bending stiffness matrices
$[A_a]$, $[A_x]$, $[A_y]$	=	aerodynamic influence matrices
C_a	=	aerodynamic damping coefficient ($C_a \approx \mu/M_\infty$ for $M_\infty \gg 1$)
$\mathbf{F}$	=	state transition matrix
$[G]$	=	aerodynamic damping matrix
g_a	=	aerodynamic damping
h	=	panel thickness
$[K_{b\phi}]$	=	coupled bending and electrical stiffness matrix
$[K_L]$	=	linear stiffness matrix
$[\bar{K}_L]$	=	linear modal stiffness matrix
$[K_{\mathrm{NL}}]$	=	nonlinear stiffness matrix
$[\bar{K}_{qq}]$	=	nonlinear modal stiffness matrix
$[K1]$, $[K2]$	=	system first-order and second-order nonlinear stiffness matrices
$[\bar{M}]$	=	modal mass matrix
$\mathbf{Q}$	=	symmetric positive semidefinite state weighting matrix
$[\bar{Q}]$	=	transformed lamina reduced-stiffness matrix
$\mathbf{Q_e}$, $\mathbf{R_e}$	=	covariance matrices
$\{q^s\}$	=	sensor charge output vector
$\mathbf{R}$	=	symmetric positive definite control effort weighting matrix.
$\mathbf{U}$	=	control input
u, v	=	in-plane displacements
V_i	=	constant electrical voltage over the ith piezoelectric layer
V_∞	=	freestream airflow speed
$\{W\}$	=	system node degrees-of-freedom vector
w	=	transverse displacement
$\mathbf{X}$, $\hat{\mathbf{X}}$	=	actual and estimate state vectors
$\mathbf{Y}$, $\hat{\mathbf{Y}}$	=	sensor output and estimate output vectors
$\{\varepsilon\}$	=	bending strain vector
$\{\varepsilon^o\}$	=	in-plane strain vector
$\{\kappa\}$	=	curvature vector
Λ	=	airflow yaw angle
λ	=	nondimensional dynamic pressure
μ	=	air-panel mass ratio
ρ	=	mass density
$\{\sigma\}$	=	stress vector
$[\Phi]$	=	eigenvector matrix
ω_o	=	reference frequency

Subscripts

a	=	air
b	=	bending
cr	=	critical
m	=	membrane
NB	=	stiffness matrices due to $\{N_b\}$
Nm	=	stiffness matrices due to $\{N_m\}$
np	=	total number of piezoelectric layers per element
ϕ	=	electrical

Received 31 July 2007; revision received 30 September 2007; accepted for publication 1 October 2007.

*Research Assistant, Department of Aerospace Engineering; mymhkim@gmail.com. Student Member AIAA.

†Research Assistant, Department of Aerospace Engineering; verdantqq@hotmail.com.

‡Professor, Department of Mechanical Engineering; jhuang@odu.edu. AIAA Member.

§Professor, Department of Aerospace Engineering; cmei@odu.edu. AIAA Associate Fellow.

I. Introduction

THE coupled equations of motion of nonlinear panel flutter at supersonic speeds have been established by using the finite

element method in structural node degrees of freedom (DOF). From an understanding of dynamic characteristics of vibration, a modal analysis of using eigenvectors has been suggested. It could afford to reduce the large number of DOF in structural nodes to a set of fewer numbers of DOF in vacuo natural modal coordinates to analyze panel vibration response behaviors [1,2]. It has been established that six (or 6×1) in vacuo natural modes (NMs) are necessary to have limit–cycle oscillations (LCO) converged for isotropic plates at zero flow yaw angle [2,3]. For laminated anisotropic composite plates, 36 (or 6×6) or fewer NMs are needed for accurate LCO flutter response [4]. Recently, the aeroelastic mode (AEM) has been introduced, which would give much smaller number of equations for LCO analysis than the traditional NMs [5,6]. It has been validated that instead of using 36 (or 6×6) NMs it could be reduced into two or six to seven AEMs for converged LCO of isotropic and laminated composite plates at zero or nonzero flow yaw angle. All four types of panel behaviors, such as flat and stable, aerothermally buckled but dynamically stable, LCO, and chaos, have been simulated with the system equations of motion in aeroelastic modal coordinates [6].

An active control of linear panel flutter was first studied with a linear quadratic regulator (LQR) full-state feedback by Scott and Weisshaar [7]. They evaluated the effectiveness of different smart materials and their placement on the panel. Surace et al. [8] developed the singular value robust control methodology to suppress flutter of composite plates based on the linear piston theory for the aerodynamic loading. Frampton et al. [9] performed the linearized potential flow aerodynamics for full transonic and supersonic speeds. The collocated direct rate feedback control method was suggested for the suppression of flutter motion. Zhou et al. [10] achieved the interaction between electrical and structural equations based on six NMs modal reduction for isotropic plates bonded with piezoelectric actuators. They also investigated the symmetric and anisotropic laminated composite plates subject to thermal loads, and studied suppression of the flutter response using the linear quadratic regulator. Doengi et al. [11] performed the output feedback regulator by placing piezoelectric self-sensing adaptive actuators on isotropic plates. They showed that λ_{cr} could be increased as high as two times. Abdel-Motagaly et al. [4,12] investigated the influence of an arbitrary yawed flow angle on LCO characteristics and found that the large number of in vacuo NMs was needed for converged LCO for isotropic and laminated composite plates. And they have studied suppression of panel flutter using 25 NMs. However, Abdel-Motagaly [4] pointed out the limitation of a simple controller due to the need for sensing the large number of state variables, and it is difficult to design optimal state feedback gains resulting from a lack of precisely estimated state values. Moon and Kim [13] studied the suppression of LCO for symmetric composite panels under a temperature effect using six NMs, and they used the hybrid active and passive piezoelectric controller. Recently, Moon et al. [14] performed the full-state feedback linearization controller for suppression panel flutter with a thermal influence using six NMs. The controller they developed considered nonlinear characteristics of structural behaviors using pseudoinverse in determining control inputs caused by an underactuated system.

Meanwhile, using in vacuo NMs still has the disadvantage of having the large number of modes for arbitrary yawed flow angles and laminated composite panels. That is because the large size of system matrices causes computational problems in optimizing feedback gains for panel flutter suppression. Guo et al. [15] studied the suppression of nonlinear panel flutter using a small number of AEMs and shape memory alloys. They compared flutter behaviors of traditional composite plates with shape memory alloy embedded hybrid composite (SMAHC) plates, and showed that SMAHC plates enabled to enlarge the desired flat and stable operational region. The present paper is the first to apply the small number of aeroelastic modes on an active control of nonlinear panel flutter using self-sensing piezoelectric actuators. Numerical simulation examples are shown for three-dimensional isotropic and composite plates at zero and nonzero yawed flow angles. The von Karman nonlinear strain–displacement relations, quasi-steady first-order piston for the aerodynamic pressure, classic laminated composite plate, and linear piezoelectricity constitutive relations theories are employed for the coupled electrical–structural finite element formulation of nonlinear panel flutter at supersonic speeds. The system equations of motion are then transformed into a set of linear aeroelastic modal coordinates with the substantially reduced number of DOF. The PZT5A [16,17] and macrofiber composite (MFC) [18] piezoelectric self-sensing actuators are bonded on isotropic plates and embedded into composite plates, respectively. Optimal shapes and locations of piezoelectric sensors and actuators are determined from the norms of feedback control gain [10] (NFCG) and the norms of Kalman filter estimation gain [12] (NKFEG) methods, respectively. As for a practical controller design, the LQR and the extended Kalman filter (EKF) are used to obtain correct state variables and generate real signals. Simulated results show that the designed LQR/EKF active controller based on AEM coordinates can successfully suppress LCO response.

II. Finite Element Formulation

A. System Equations of Motion in Structure Node DOF

Governing system equations of motion for nonlinear panel flutter are derived for thin flat composite plates with embedded piezoelectric actuators. The Bogner–Fox–Schmit (BFS) rectangular C^1 conforming plate element [19] is considered. The nodal DOF of each element are composed of 16 bending $\{w_b\}$, 8 in-plane $\{w_m\}$, and an additional electrical DOF, $\{w_\phi\}$, for a corresponding pair of piezoelectric actuator and sensor patches. The von Karman large deflection strain–displacement relations are adopted and the classical laminated plate theory is used as follows:

$$\{\varepsilon\} = \begin{Bmatrix} u_{,x} \\ v_{,y} \\ u_{,y} + v_{,x} \end{Bmatrix} + \frac{1}{2}\begin{Bmatrix} w_{,x}^2 \\ w_{,y}^2 \\ 2w_{,x}w_{,y} \end{Bmatrix} + z\begin{Bmatrix} -w_{,xx} \\ -w_{,yy} \\ -2w_{,xy} \end{Bmatrix} = \begin{Bmatrix} \varepsilon_m^o \end{Bmatrix} + \begin{Bmatrix} \varepsilon_b^o \end{Bmatrix} + z\begin{Bmatrix} \kappa \end{Bmatrix} = \{\varepsilon^o\} + z\{\kappa\} \tag{1}$$

where a comma indicates a derivative in terms of the subscript. The electrical DOF over each piezoelectric layer is generated with the constant potential voltage, and the electrical field $\{E\}$ can be determined with respect to the electrical DOF $\{w_\phi\}$ given by

$$\begin{Bmatrix} E_1 \\ \vdots \\ E_{\text{np}} \end{Bmatrix} = -[B_\phi]\{w_\phi\} = -\begin{bmatrix} \frac{1}{h_1} & \cdots & 0 \\ \vdots & \ddots & \vdots \\ 0 & \cdots & \frac{1}{h_{\text{np}}} \end{bmatrix}\begin{Bmatrix} V_1 \\ \vdots \\ V_{\text{np}} \end{Bmatrix} \tag{2}$$

where h_k is the thickness of the kth piezoelectric layer, and the polarization of isotropic piezoelectric materials is generated in the 3-direction. The resultant force and moment per unit length are calculated from integrating the stress vector over the laminate thickness with embedded piezoelectric layers. The constitutive equations are expressed by

$$\begin{Bmatrix} N \\ M \end{Bmatrix} = \begin{bmatrix} A & B \\ B & D \end{bmatrix}\begin{Bmatrix} \varepsilon^o \\ \kappa \end{Bmatrix} - \begin{Bmatrix} N_\phi \\ M_\phi \end{Bmatrix}$$
$$(\{N_\phi\}, \{M_\phi\}) = \int_{-h/2}^{h/2} [\bar{Q}]_k \{d\}_k E_{ik}(1, z)\, \mathrm{d}z \tag{3}$$

$$([A], [B], [D]) = \int_{-h/2}^{h/2} [\bar{Q}]_k (1, z, z^2)\, \mathrm{d}z \tag{4}$$

The piezoelectric charge constant in the principal axes is $\{d\}_k^T = [d_{31}, d_{32}, 0]$, $d_{32} = d_{31}$ and $i = 3$ for PZT5A or $\{d\}_k^T = [d_{11}, d_{12}, 0]$ and $i = 1$ for MFC actuators [18]. For a conventional composite layer, simply set $E_{ik} = \{d\}_k = 0$. The first subscript position refers to the direction of the electric field and the second refers to the direction of the piezoelectric induced strain. In this study, the in-plane piezoelectric actuation force $\{N_\phi\}$ is neglected because the bending moment $\{M_\phi\}$ induced from piezoelectric

actuators is much more efficient in the suppression of flutter motion [10,12]. The bending moment is produced by applying equal and opposite voltage to a pair of the top and bottom piezoelectric layers for each element, which act as an electrical DOF, $\{w_\phi\}$. The aerodynamic pressure is prescribed with the quasi-steady first-order piston theory at supersonic speeds ($1.6 < M_\infty < 5$). The transverse displacement of skin panels of a flight vehicle is associated with the aerodynamic loading given by [1,3,4,12]

$$\begin{aligned}\Delta p_a &= \frac{-2q_a}{\beta}\left[w_{,x}\cos\Lambda + w_{,y}\sin\Lambda + \left(\frac{M_\infty^2-2}{M_\infty^2-1}\right)\frac{1}{V_\infty}\frac{\partial w}{\partial t}\right] \\ &= -\left[\lambda\frac{D_{110}}{a^3}(w_{,x}\cos\Lambda + w_{,y}\sin\Lambda) + \frac{g_a}{\omega_o}\frac{D_{110}}{a^4}\frac{\partial w}{\partial t}\right] \end{aligned} \tag{5}$$

where $q_a = \rho_a V_\infty^2/2$ is the dynamic pressure, $\beta = \sqrt{M_\infty^2 - 1}$, $\omega_o = \sqrt{D_{110}/\rho h a^4}$, and D_{110} is the first entry component of the laminate bending stiffness matrix obtained by placing all fibers of the composite layers in x direction. The nondimensional parameters are written by

$$\begin{aligned}\lambda &= \frac{2q_a a^3}{\beta D_{110}}, \qquad g_a = \frac{\rho_a V_\infty (M_\infty^2-2)}{\rho h \omega_o \beta^3} = \sqrt{\lambda C_a} \\ \mu &= \frac{\rho_a a}{\rho h}, \qquad C_a = \left(\frac{M_\infty^2-2}{M_\infty^2-1}\right)^2\frac{\mu}{\beta}\end{aligned} \tag{6}$$

The coupled electrical and structural nonlinear equations of motion for a laminated composite plate with embedded piezoelectric layers are derived based on the Hamilton's principle and finite element expressions. Standard procedures of assembling element matrices are applied with kinematic boundary conditions to obtain system equations of motion for nonlinear panel flutter with piezoelectric self-sensing actuators [11,12] as follows.

Actuator equation in structure node DOF:

$$\begin{aligned}&\begin{bmatrix}[M_b] & 0\\ 0 & [M_m]\end{bmatrix}\begin{Bmatrix}\ddot{W}_b\\ \ddot{W}_m\end{Bmatrix} + \begin{bmatrix}[G] & 0\\ 0 & 0\end{bmatrix}\begin{Bmatrix}\dot{W}_b\\ \dot{W}_m\end{Bmatrix} \\ &+ \left(\lambda\begin{bmatrix}[A_x]\cos\Lambda + [A_y]\sin\Lambda & 0\\ 0 & 0\end{bmatrix} + \begin{bmatrix}[K_b] & [K_{bm}]\\ [K_{mb}] & [K_m]\end{bmatrix}\right. \\ &\left. + \begin{bmatrix}[K1_{\mathrm{Nm}}] + [K1_{\mathrm{NB}}] & [K1_{bm}]\\ [K1_{mb}] & 0\end{bmatrix} + \begin{bmatrix}[K2] & 0\\ 0 & 0\end{bmatrix}\right)\begin{Bmatrix}W_b\\ W_m\end{Bmatrix} \\ &= -\begin{bmatrix}[K_{b\phi}]\\ 0\end{bmatrix}\{W_\phi\}\end{aligned} \tag{7}$$

Sensor equation in structure node DOF:

$$\{q^s\} = -[[K_{\phi b}]\ \ 0]\begin{Bmatrix}W_b\\ W_m\end{Bmatrix} \tag{8}$$

The structure node DOF vector consists of the bending and in-plane displacements, $\{W\} = \{W_b, W_m\}^T$. The first- and second-order nonlinear stiffness matrices, $[K1]$ and $[K2]$, are the linear and quadratic function of unknown displacements $\{W\}$, respectively. It is noted that for isotropic and symmetrically laminated composite plates, the coupling matrix of bending and in-plane $[B]$ equals zero. This leads some substiffness matrices $[K_{mb}]$, $[K_{bm}]$, and $[K1_{NB}]$ to be void. The aforementioned actuator equation provides a relation between the actuator voltage and the panel response. Meanwhile, the sensor equation generates the voltage signal obtained in proportion to the displacement. In Eq. (7), the in-plane inertial term is neglected due to high frequencies of in-plane motion. Thus, the in-plane displacement can be driven in association with the bending displacement vector as

$$\{W_m\} = -[K_m]^{-1}[K1_{mb}]\{W_b\} \tag{9}$$

The actuator and sensor equations can be rearranged in terms of the bending displacement as

$$[M_b]\{\ddot{W}_b\} + [G]\{\dot{W}_b\} + ([K_L] + [K_{\mathrm{NL}}])\{W_b\} = -[K_{b\phi}]\{W_\phi\} \tag{10}$$

$$\{q^s\} = -[K_{\phi b}]\{W_b\} \tag{11}$$

where the linear and nonlinear stiffness matrices are expressed by

$$[K_L] = \lambda([A_x]\cos\Lambda + [A_x]\sin\Lambda) + [K_b] \tag{12}$$

$$[K_{\mathrm{NL}}] = [K1_{Nm}] + [K2] - [K1_{bm}][K_m]^{-1}[K1_{mb}] \tag{13}$$

The size of the system mass $[M_b]$ and linear stiffness $[K_L]$ matrices is usually too large to be tractable. It remains an extremely small time step that consumes laborious computation in a numerical simulation. In addition, at every time step the nonlinear stiffness matrix $[K_{\mathrm{NL}}]$ needs to be evaluated and updated. To handle these problems, the modal reduction approach with fewer numbers of modes is presented in this study. By transforming the equations of motion, Eqs. (10) and (11), into a set of a smaller number of modal coordinates, it not only reduces the size of the system equations, but it also increases the time step of numerical integration.

B. Equations of Motion in Aeroelastic Modal Coordinates

Traditionally, the in vacuo NMs are employed in developing the coupled nonlinear modal equations [1–4,7,10,12–14]. Most recently, AEMs have been introduced and used for nonlinear panel flutter analysis at an arbitrary flow-yawed angle [5] and elevated temperature [6], as well as flutter suppression using shape memory alloys [15]. Previous research has shown [5,6,15] the great reduction in number of modes from 36 (or 6×6) NMs to six or seven AEMs for nonorthotropic laminated composite plates at zero or nonzero flow yaw angle, and from six (or 6×1) NMs to two AEMs for isotropic or laminated orthotropic panels for flutter analysis. Consequently, the application of using AEMs is emphasized in this paper for the ease of designing active controllers and for reducing computational time. It is assumed that the bending displacement of panels can be represented as linear combinations of some known AEMs defined as

$$\{W_b\} = \sum_{r=1}^{n} q_r(t)\{\phi_r\} = [\Phi_R]\{q\} \tag{14}$$

where n is the number of AEMs and the maximum component of the rth right eigenvector $\{\phi_r\}$ is normalized to unity. The modal matrix $[\Phi_R]$ consists of selected aeroelastic modes. The AEMs and corresponding frequencies are determined under the linear stiffness matrix combined with the aerodynamic influence matrix in an eigenvalue problem given as

$$\omega_r^2[M_b]\{\phi_r\} = ([K_b] + \lambda_o[A_a])\{\phi_r\} \tag{15}$$

The aerodynamic matrix $[A_a]$ represents $[A_x]\cos\Lambda + [A_y]\sin\Lambda$ taking yawed angles into account, and the λ_o is a preselected value, $\lambda_o < \lambda_{\mathrm{cr}}$. It has been substantiated that the selected nondimensional dynamic pressure λ_o within 10% below λ_{cr} is reasonably acceptable [5]. Because of the skew symmetric aerodynamic matrix $[A_a]$, the right and left eigenvectors [20] are adopted to derive aeroelastic (AE) modal equations of motion. The nonlinear stiffness matrices in Eq. (13) can be directly calculated based on corresponding element components $\{w_b\}^{(r)}$ from the known system $\{\phi_r\}$ and expressed as

$$[K1_{mb}] = \sum_{r=1}^{n} q_r[K1_{mb}]^{(r)}, \qquad [K2] = \sum_{r=1}^{n}\sum_{s=1}^{n} q_r q_s[K2]^{(rs)} \tag{16}$$

where superindices denote the corresponding mode shape. Thus, the nonlinear modal stiffness $[K1_{mb}]^{(r)}$ and $[K2]^{(rs)}$ matrices become constant known values. The nonlinear stiffness matrix $[K1_{Nm}]$ is dependent on $\{W_m\}$, and the in-plane displacement $\{W_m\}$ expressed

in Eq. (9) can be written as [5]

$$\{W_m\} = -[K_m]^{-1}\left(\sum_{r=1}^{n} q_r[K1_{mb}]^{(r)}\right)[\Phi_R]\{q\}$$
$$= -\sum_{r=1}^{n}\sum_{s=1}^{n} q_r q_s\{\phi_{rs}\}_m \tag{17}$$

The in-plane mode shape $\{\phi_{rs}\}_m$ developed by corresponding AEMs $\{\phi_r\}$ and $\{\phi_s\}$ and the nonlinear stiffness $[K1_{Nm}]$ matrix are

$$\{\phi_{rs}\}_m = [K_m]^{-1}[K1_{mb}]^{(r)}\{\phi_s\}$$
$$[K1_{\mathrm{Nm}}] = -\sum_{r=1}^{n}\sum_{s=1}^{n} q_r q_s[K2_{Nm}]^{(rs)} \tag{18}$$

After the modal transfer, $[K1_{Nm}]$ has of quadratic dependency on AEMs' coordinates q_r and q_s and $[K2_{Nm}]^{(rs)}$ becomes a constant matrix as well. The modal mass, aerodynamic damping, linear stiffness matrices, and cubic nonlinear modal stiffness matrices are transformed with left and right eigenvectors as

$$([\bar{M}_b],[\bar{G}],[\bar{K}_L]) = [\Phi_L]^T([M_b],[G],[K_L])[\Phi_R]$$
$$[\bar{K}_{b\phi}] = [\Phi_L]^T[K_{b\phi}] \qquad [\bar{K}_{\phi b}] = [K_{\phi b}][\Phi_R] \tag{19}$$

$$[\bar{K}_{qq}]\{q\} = [\Phi_L]^T\sum_{r=1}^{n}\sum_{x=1}^{n} q_r q_s([K2]^{(rs)} - [K2_{Nm}]^{(rs)}$$
$$- [K1_{bm}]^{(r)}[K_m]^{-1}[K1_{mb}]^{(s)})[\Phi_R]\{q\} \tag{20}$$

The left eigenvector matrix $[\Phi_L]$ is composed of the certain chosen AEMs. Notice that $[\Phi'_L]$ (square matrix) has a relation with the original right eigenvector matrix $[\Phi'_R]$ as $[\Phi'_L]^T = [\Phi'_R]^{-1}$. The left eigenvector $[\Phi_L]$ can be then established by extracting the corresponding part from the $[\Phi'_R]^{-1}$ [20]. The equations of motion based on AEM coordinates are given by the following.

Actuator equation, Eq. (10), in AEM coordinates becomes

$$[\bar{M}_b]\{\ddot{q}\} + [\bar{G}]\{\dot{q}\} + ([\bar{K}_L] + [\bar{K}_{qq}])\{q\} = -[\bar{K}_{b\phi}]\{W_\phi\} \tag{21}$$

Sensor equation, Eq. (11), in AEM coordinates becomes

$$\{q^s\} = -[\bar{K}_{\phi b}]\{q\} \tag{22}$$

A modal participation determines which mode and how many modes are required for the accurate converged LCO solution and it is defined as [5]

$$\text{Participation of the } r\text{th mode} = \frac{\max|q_r|}{\sum_{s=1}^{n}\max|q_s|} \tag{23}$$

Because of the added aerodynamic influence matrix in Eq. (15), the AE mode shape has an analogous configuration to the deflection shape of the LCO dynamic response as shown in Fig. 1 for a simply supported isotropic square plate. This characteristic of AEMs clearly indicates that very few (only two for this case) modes are needed for nonlinear panel flutter analysis.

III. Control Design Scheme

In the purpose of the pragmatic realistic controller, the LQR accompanied by the EKF is presented to suppress panel flutter motion. Accurately obtained feedback states can be taken through the EKF estimator considering a nonlinear system model by which robustness of a regulator can be increased. For designing output feedback controllers, the system equations of motion in AEM coordinates, Eqs. (21) and (22), can be cast into the standard state-space representation form as follows:

$$\dot{\mathbf{X}} = \bar{\mathbf{A}}\mathbf{X} + \mathbf{B}\mathbf{U} \qquad \mathbf{Y} = \mathbf{C}\mathbf{X} + \mathbf{D}\mathbf{U} \tag{24}$$

where

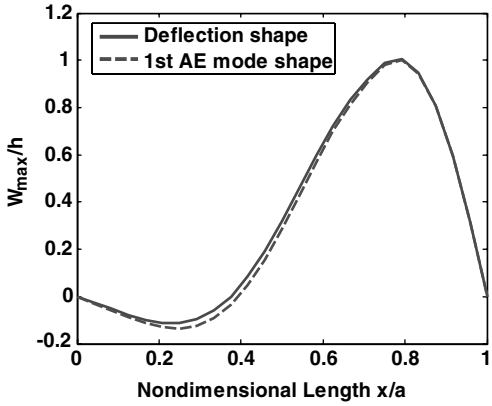

Fig. 1 Normalized AE mode and LCO deflection for a simply supported isotropic square plate at $\lambda = 800$ and $\Lambda = 0$ deg.

$$\mathbf{X} = \begin{Bmatrix} q \\ \dot{q} \end{Bmatrix}, \qquad \mathbf{U} = \{W_\phi\}, \qquad \mathbf{Y} = \{q^s\} \tag{25}$$

The system state matrices supply the information about an input–output relationship as follows:

$$\bar{\mathbf{A}} = \mathbf{A} + \mathbf{A_o} = \begin{bmatrix} 0 & \mathbf{I} \\ -[\bar{M}_b]^{-1}[\bar{K}_L] & -[\bar{M}_b]^{-1}[\bar{G}] \end{bmatrix}$$
$$+ \begin{bmatrix} 0 & 0 \\ -[\bar{M}_b]^{-1}[\bar{K}_{qq}] & 0 \end{bmatrix}$$
$$\mathbf{B} = \begin{bmatrix} 0 \\ -[\bar{M}_b]^{-1}[\bar{K}_{b\phi}] \end{bmatrix}, \qquad \mathbf{C} = [-[\bar{K}_{\phi b}] \;\; 0], \qquad \mathbf{D} = 0 \tag{26}$$

The system state matrix $\bar{\mathbf{A}}$ consists of the linear $\mathbf{A}$ and nonlinear $\mathbf{A_o}$ parts. By neglecting higher-order terms in the Tayer series, the linearization of the system matrix is simply $\mathbf{A}$, which is used for modern optimal control laws in the following LQR design. The outline of contriving a controller is separated into two parts, the state feedback and the state estimation, respectively. The state feedback is executed with estimated states $\hat{\mathbf{X}}$ observed from the EKF as

$$\mathbf{U} = -\mathbf{K}\hat{\mathbf{X}} \tag{27}$$

The optimal gain $\mathbf{K}$ matrix of the LQR controller can be determined based on minimizing a quadratic performance index $\mathbf{J}$, which is associated with the state and input control effort.

$$\mathbf{J} = \int_0^\infty [\mathbf{X^T Q X} + \mathbf{U^T R U}]\,\mathrm{d}t \tag{28}$$

$$\mathbf{K} = \mathbf{R^{-1}B^T P} \tag{29}$$

The positive definite symmetric matrix $\mathbf{P}$ can be calculated from the solution of the algebraic Riccati equation given by

$$\mathbf{A}^{\mathbf{T}}\mathbf{P} + \mathbf{P}\mathbf{A} - \mathbf{P}\mathbf{B}\mathbf{R}^{-1}\mathbf{B}^{\mathbf{T}}\mathbf{P} + \mathbf{Q} = \mathbf{0} \tag{30}$$

In the EKF [12,21], the state estimator is improved by keeping the modal nonlinear stiffness matrices. The nonlinear state estimation and measurement are given as

$$\dot{\hat{\mathbf{X}}} = \bar{\mathbf{A}}(\hat{\mathbf{X}}, \mathbf{t})\hat{\mathbf{X}} + \mathbf{B}\mathbf{U} + \mathbf{K_e}(\mathbf{t})(\mathbf{Y} - \mathbf{C}\hat{\mathbf{X}}), \qquad \hat{\mathbf{Y}} = \mathbf{C}\hat{\mathbf{X}} \tag{31}$$

In applying Tayor's series [21], the first-order linear approximation coefficients can be described as

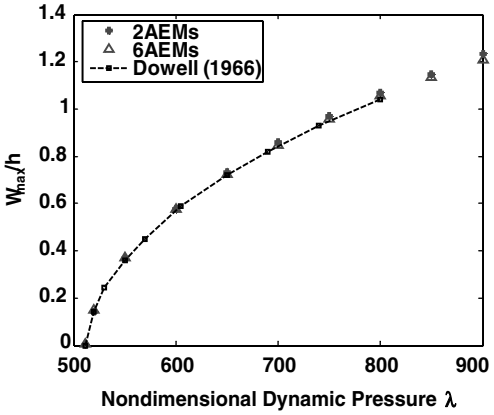

Fig. 2 Comparison of LCO displacement using two AEMs, six NMs, and a PDE/Galerkin for a simply supported isotropic square plate at $\Lambda = 0$ deg.

$$\mathbf{F}(\mathbf{t}) \approx \left.\frac{\partial \mathbf{f}(\mathbf{X},\mathbf{t})}{\partial \mathbf{X}}\right|_{\mathbf{X}=\hat{\mathbf{X}}(\mathbf{t})} = \left[\begin{array}{ccccc} \frac{\partial \mathbf{f_1}}{\partial \mathbf{X_1}} & \frac{\partial \mathbf{f_1}}{\partial \mathbf{X_2}} & \frac{\partial \mathbf{f_1}}{\partial \mathbf{X_3}} & \cdots & \frac{\partial \mathbf{f_1}}{\partial \mathbf{X_n}} \\ \frac{\partial \mathbf{f_2}}{\partial \mathbf{X_1}} & \frac{\partial \mathbf{f_2}}{\partial \mathbf{X_2}} & \frac{\partial \mathbf{f_2}}{\partial \mathbf{X_3}} & \cdots & \frac{\partial \mathbf{f_2}}{\partial \mathbf{X_n}} \\ \frac{\partial \mathbf{f_3}}{\partial \mathbf{X_1}} & \frac{\partial \mathbf{f_3}}{\partial \mathbf{X_2}} & \frac{\partial \mathbf{f_3}}{\partial \mathbf{X_3}} & \cdots & \frac{\partial \mathbf{f_1}}{\partial \mathbf{X_n}} \\ \vdots & \vdots & \vdots & \ddots & \vdots \\ \frac{\partial \mathbf{f_n}}{\partial \mathbf{X_1}} & \frac{\partial \mathbf{f_n}}{\partial \mathbf{X_2}} & \frac{\partial \mathbf{f_n}}{\partial \mathbf{X_3}} & \cdots & \frac{\partial \mathbf{f_n}}{\partial \mathbf{X_n}} \end{array}\right]_{\mathbf{X}=\hat{\mathbf{X}}(\mathbf{t})} \tag{32}$$

where

$$\mathbf{f}(\mathbf{X},\mathbf{t}) = \dot{\mathbf{X}} = \bar{\mathbf{A}}(\mathbf{X},\mathbf{t})\mathbf{X} + \mathbf{BU}$$
$$\mathbf{X} = [\mathbf{X_1}\ \ \mathbf{X_2}\ \ \mathbf{X_3}\ \ \cdots\ \ \mathbf{X_n}]^{\mathbf{T}} \tag{33}$$

The linearization technique is adopted over the estimated trajectory rather than the predefined nominal trajectory. It allows deviation between the estimated trajectory and the actual trajectory to remain in sufficiently small ranges.

$$\mathbf{F}(\mathbf{t}) \approx \mathbf{A} + \left[\mathbf{A_o}(\mathbf{X},\mathbf{t}) + \frac{\partial \mathbf{A_o}(\mathbf{X},\mathbf{t})}{\partial \mathbf{X}}\mathbf{X}\right]\Bigg|_{\mathbf{X}=\hat{\mathbf{X}}(\mathbf{t})} \tag{34}$$

The Kalman optimal filter gain $\mathbf{K_e}$ can be computed at every time interval resulting from solving the differential Riccati equation as follows:

$$\dot{\mathbf{P}}_{\mathbf{e}}(\mathbf{t}) = \mathbf{F}(\mathbf{t})\mathbf{P_e}(\mathbf{t}) + \mathbf{P_e}(\mathbf{t})\mathbf{F}(\mathbf{t})^{\mathbf{T}} - \mathbf{P_e}(\mathbf{t})\mathbf{C}^{\mathbf{T}}\mathbf{R_e^{-1}}\mathbf{C}\mathbf{P_e}(\mathbf{t}) + \mathbf{Q_e} \tag{35}$$

$$\mathbf{K}_{\mathbf{e}}(\mathbf{t}) = \mathbf{P_e}(\mathbf{t})\mathbf{C}^{\mathbf{T}}\mathbf{R_e^{-1}} \tag{36}$$

Along with preceding equations, the optimal location of actuators is determined by the norms of feedback gain designed for the LQR regulator in Eq. (29) and the optimal location of sensors is obtained by the norms of feedback gain designed for the EKF filter [10–12] in Eq. (36).

$$\mathbf{NFCG} = \|\mathbf{K_{LQR}}\|_2, \qquad \mathbf{NKFEG} = \|\mathbf{K_{Kalman}}\|_2 \tag{37}$$

IV. Numerical Results

The designed LQR controller with the EKF estimator is performed to suppress large-amplitude nonlinear panel flutter for three different systems: an isotropic square plate at zero yaw angle and a rectangular

Table 1 Modal participation values using AEMs and NMs for a simply supported isotropic square plate at $\Lambda = 0$ deg

		Modal participation, %					
W_{max}/h	Modes	q_{11}	q_{21}	q_{31}	q_{41}	q_{51}	q_{61}
0.57	AEM	63.93	34.83	0.91	0.21	0.08	0.04
	NM	42.12	38.91	11.2	4.81	1.93	1.03
1.07	AEM	67.32	29.43	1.51	1.16	0.44	0.14
	NM	30.12	49.96	11.53	6.21	0.80	1.38

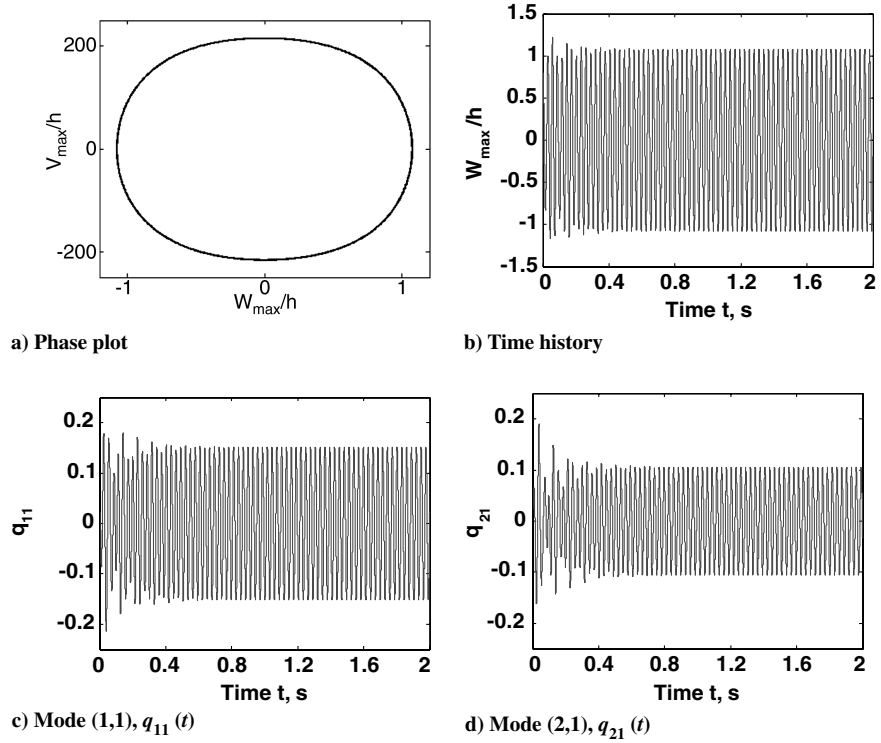

a) Phase plot

b) Time history

c) Mode (1,1), $q_{11}(t)$

d) Mode (2,1), $q_{21}(t)$

Fig. 3 LCO response using two AEMs for a simply supported isotropic square plate at $\lambda = 800$ and $\Lambda = 0$ deg.

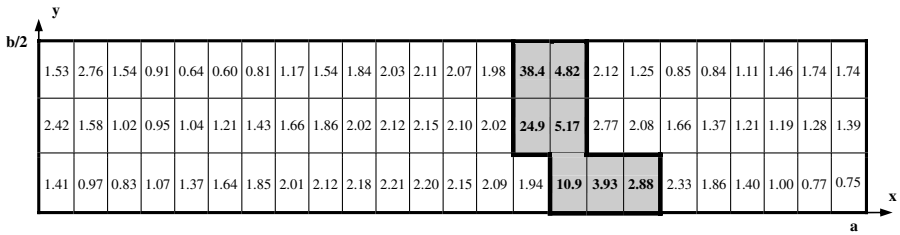

a) NFCG norm of each element for bottom half isotropic square panel using PZT5A

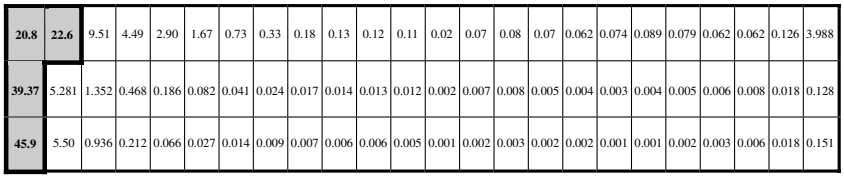

b) NKFEG norm of each element for bottom half isotropic square panel using PZT5A

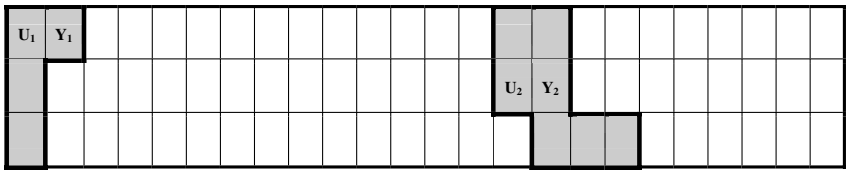

c) Final optimized placement of self-sensing actuators and sensors based on NFCG and NKFEG

Fig. 4 Optimal location of PZT5A self-sensing actuators and sensors for a simply supported bottom half isotropic square plate at $\Lambda = 0$ deg.

symmetrically laminated anisotropic composite plate at zero and nonzero yaw angles. The designed parameters of $\mathbf{Q}$ and $\mathbf{R}$ weighting matrices for the controller and $\mathbf{Q_e}$ and $\mathbf{R_e}$ weighting matrices for the estimator are chosen as follows:

$$\mathbf{Q} = c \times \rho h \times \begin{bmatrix} \omega_r & 0 \\ 0 & \omega_r \end{bmatrix}, \qquad \mathbf{R} = c \times [\mathbf{I}] \tag{38}$$

$$\mathbf{Q_e} = c \times [\mathbf{I}], \qquad \mathbf{R_e} = [\mathbf{C}][\mathbf{C}]^T \tag{39}$$

where ω_r $(r = 1, 2, 3 \cdots n)$ are linear frequencies of AEMs, and c is a constant number. For the simply supported isotropic square plate of $28 \times 28 \times 0.054$ in. at $\Lambda = 0$ deg, the half-plate is modeled with 24×3 mesh because of a symmetric configuration. The aerodynamic damping C_a is set to 0.01. For the clamped rectangular

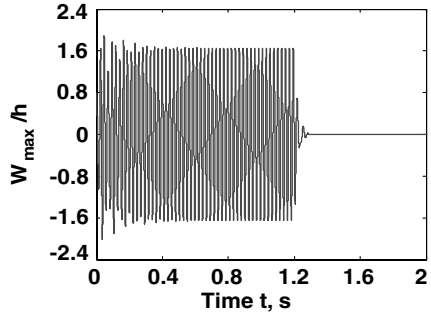

a) Controlled LCO flutter amplitude

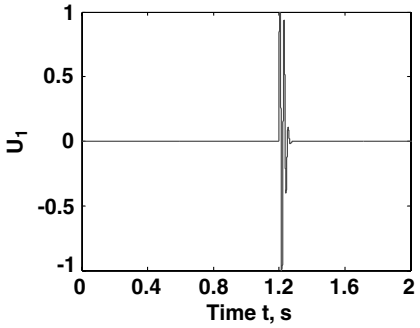

b) Control input U_1

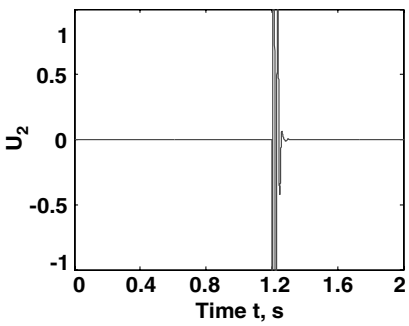

c) Control input U_2

Fig. 5 Suppression of LCO using PZT5A for a simply supported isotropic square plate at $\lambda = 1400$ and $\Lambda = 0$ deg.

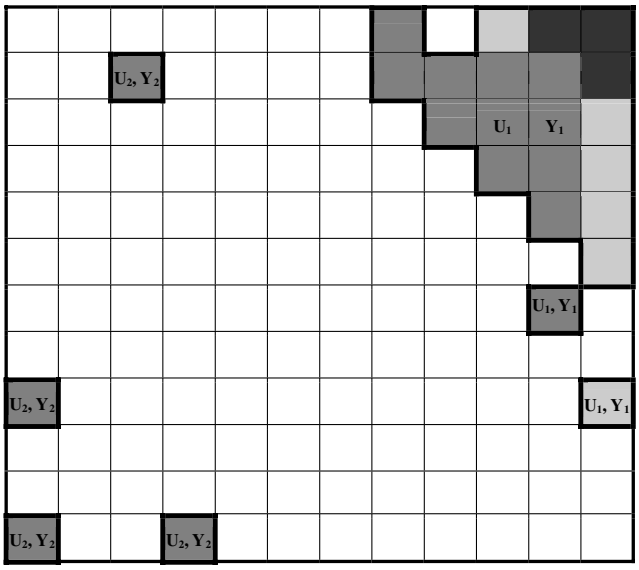

Fig. 6 Optimal location of PZT5A self-sensing actuators and sensors based on NFCG and NKFEG for a clamped rectangular $[-40/40/-40]$ composite plate at $\Lambda = 0$ deg.

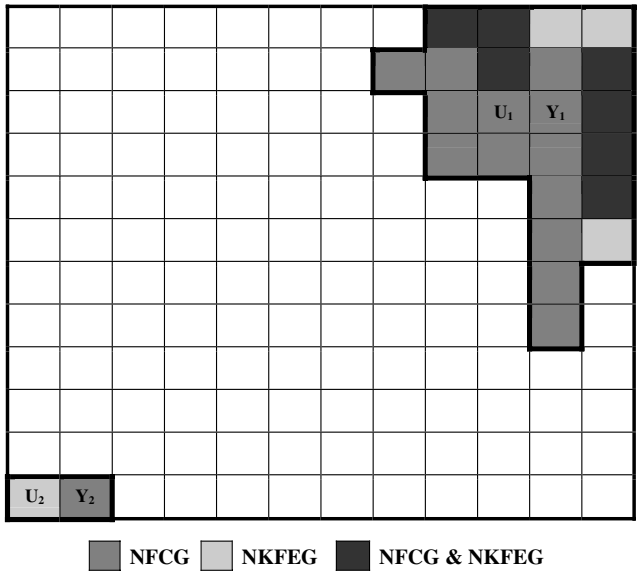

Fig. 8 Optimal location of MFC self-sensing actuators and sensors based on NFCG and NKFEG for a clamped rectangular $[-40/40/-40]$ composite plate at $\Lambda = 0$ deg.

composite plate of $30 \times 24 \times 0.048$ in. at $\Lambda = 0$ deg and $\Lambda \neq 0$ deg, the full plate is modeled with 12×12 mesh. The three-layered graphite epoxy has a lamination of $[-40/40/-40]$. The aerodynamic damping C_a is used as 0.01. The material properties of the isotropic and composite plate, PZT5A and MFC, are shown in the Appendix, Table A1.

A. Isotropic Square Plate with Zero Yaw Angle ($\Lambda = 0$ deg)

The equations of motion in AEM coordinates, Eq. (21), are demonstrated first by using the fourth-order Runge–Kutta method in the time domain without piezoelectric actuators. It is validated that the LCO maximum deflection vs dynamic pressure λ in using two AEMs has an excellent agreement to that of using six NMs as shown in Fig. 2 for the simply supported square panel. The result based on partial differential equation (PDE)/Galerkin using six NMs by Dowell [3] is also given to make a comparison. The modal participation values in using six AEMs as well as six NMs are shown in Table 1. It evidently shows that the first two aeroelastic modes are dominant for the converged LCO amplitude. The phase and time history plots at $\lambda = 800$ are shown in Figs. 3a and 3b and the time response of modes $q_{11}(t)$ and $q_{21}(t)$ are shown in Figs. 3c and 3d.

In Fig. 4, the NFCG provides the optimal location of actuators where the norms of feedback gain $\mathbf{K} > 2.87$, and the NKFEG

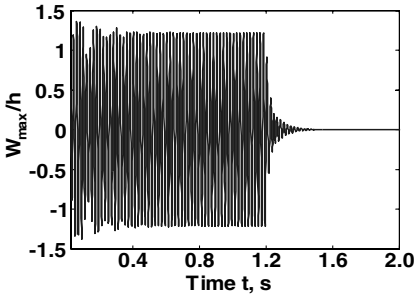

a) Controlled LCO flutter amplitude

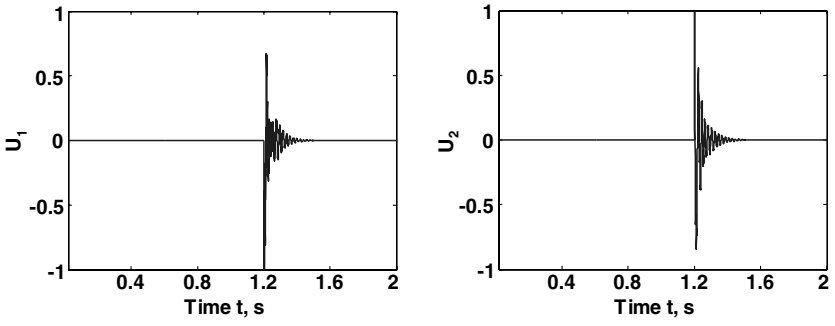

b) Control input U_1 **c) Control input U_2**

Fig. 7 Suppression of LCO using PZT5A for a clamped rectangular $[-40/40/-40]$ composite plate at $\lambda = 500$ and $\Lambda = 0$ deg.

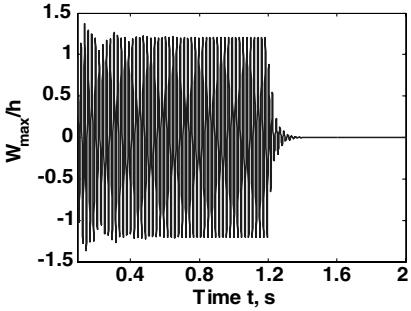

a) Controlled LCO flutter amplitude

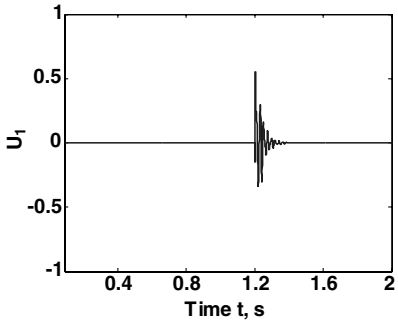

b) Control input U_1

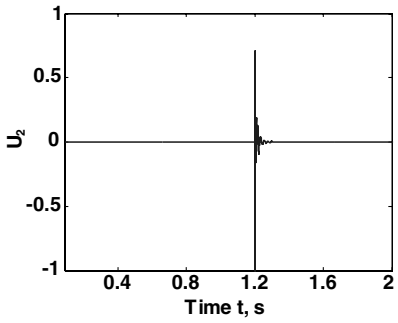

b) Control input U_2

Fig. 9 Suppression of LCO using MFC for a clamped rectangular composite plate $[-40/40/-40]$ at $\lambda = 500$ and $\Lambda = 0$ deg.

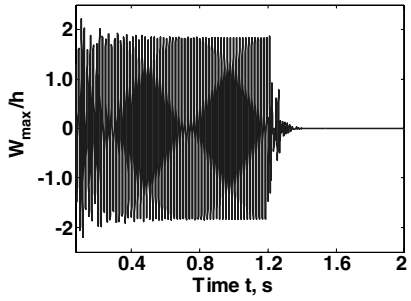

a) Controlled LCO flutter amplitude

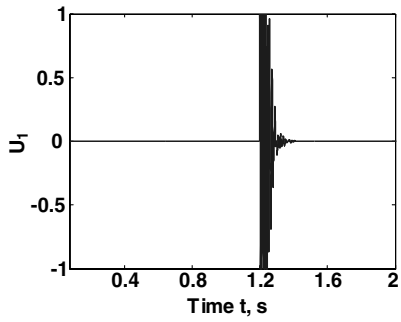

b) Control input U_1

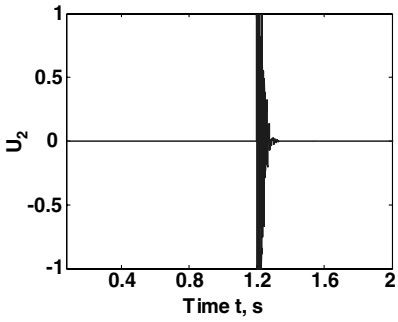

c) Control input U_2

Fig. 10 Suppression of LCO using MFC for a clamped rectangular $[-40/40/-40]$ composite plate at $\lambda = 710$ and $\Lambda = 0$ deg.

generates the optimal location for sensors where the norms of estimator gain $\mathbf{K}_e > 22.5$. The self-sensing piezoelectric actuators are bonded on the top and bottom surfaces of the isotropic panel along to the final optimal placement determined by both NFCG and NKFEG, as shown in Fig. 4c. The optimal size of the actuators is studied with less than 20% of the panel area [12]. Because of the density of piezo materials, the critical dynamic pressure λ_{cr} is slightly changed from that without piezo patches.

The control force is activated after the stable LCO response is reached. The LCO is then completely suppressed after several input cycles, as shown in Figs. 5a–5c. To evaluate the control performance, the maximum flutter-free dynamic pressure λ_{max} is adopted based on how much the LCO amplitude can be suppressed with given piezoelectric actuators [10,12]. The λ_{cr} value is changed from 512 to 612 by placing the piezo materials at the leading edge and around the maximum deflection location (see Fig. 4c). The λ_{max} is evaluated as 1551. The ratio $\lambda_{max}/\lambda_{cr}$ is 2.54 with 15.3% of the total panel area covered by self-sensing piezo actuators. The developed controller can increase the dynamic pressure up to 2.54 times the λ_{cr}.

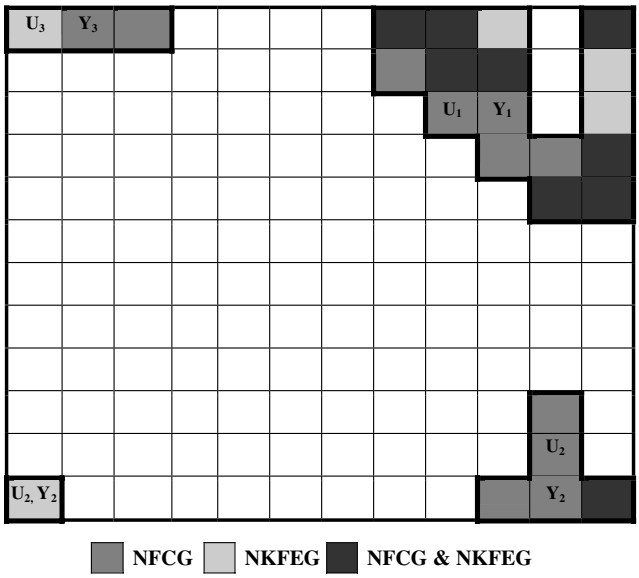

Fig. 11 Optimal location of MFC self-sensing actuators and sensors based on NFCG and NKFEG for a clamped rectangular [−40/40/ − 40] composite plate at $\Lambda = 60$ deg.

B. Composite Rectangular Plate with Zero Yaw Angle ($\Lambda = 0$ deg)

In the present work, six AEMs are employed for the converged LCO response of a laminated [−40/40/ − 40] composite plate [5]. In Fig. 6, the final optimal location is determined based on the NFCG in which the norms of feedback gain $\mathbf{K} > 12.9$, and the NKFEG in which the norms of estimator gain $\mathbf{K_e} > 93.0$. The optimal location results show a nonsymmetric configuration that is different from the isotropic plate because of the lamination angle of the composite plate. More piezo actuators or control efforts are expected to suppress the LCO because composite plates with the clamped boundary condition are stiffer than isotropic plates with the simply supported condition.

Figures 7a–7c show the successfully controlled response by using two input efforts of PZT5A actuators. For the better control performance MFC piezo actuators are employed. The size of MFC actuators is 17.4% of the whole plate area, which is the same as the size of the PZT5A actuators. The most favorable location of MFC actuators shown in Fig. 8 is slightly different from that of using PZT5A (Fig. 6), which is attributed to the fiber-reinforced composite characteristics of MFC actuators compared to the traditional isotropic ceramic PZT5A. In Fig. 8, the optimized placement for actuators is obtained from the norms of $\mathbf{K} > 14.24$ and those for sensors are from the norms of $\mathbf{K_e} > 13.78$.

The control performance of using MFC and PZT5A actuators is compared at the same level of the LCO amplitude ($W_{\max}/h$). Because the charge constant of MFC is twice as large as that of PZT5A ($d_{11} > 2d_{31}$), it generates the higher strain. From Figs. 7 and 9, the LCO deflection can be suppressed with the small control input effort by using MFC as compared to PZT5A. As for the MFC actuators, a higher maximum flutter-free dynamic pressure can be obtained. The ratio of $\lambda_{\max} = 550$ to $\lambda_{cr} = 243$ is 2.26 by using PZT5A, and the ratio of $\lambda_{\max} = 710$ to $\lambda_{cr} = 275$ is 2.61 by using MFC. Figures 10a–10c show that the LCO is completely suppressed at $\lambda_{\max} = 710$ using MFC.

C. Composite Rectangular Plate with Nonzero Yaw Angle ($\Lambda \neq 0$ deg)

The designed controller using AEMs is studied for the composite plate with a nonzero yaw angle as well. In practical consideration of the actual flight, the selected AEMs should not be changed differently for arbitrary varied yawed flow angles. After the investigation of evenly distributed AEMs over the flow angles, the limited number of AEMs can be determined for the control strategy. The optimized LQR/EKF controller is developed using seven AEMs for the clamped composite plate. The seven AEMs are selected such as follows: modes $q1$ and $q2$, the first and second AEM at $\Lambda = 0$ deg; modes $q3$ and $q4$, the first and second AEM at $\Lambda = 90$ deg; $q5$, the first AEM at $\Lambda = 22.5$ deg; $q6$, the first AEM at $\Lambda = 45$ deg; and $q7$, the first AEM at $\Lambda = 67.5$ deg [5]. Therefore, the given set of seven AEMs will cover all possible flow angles. In Fig. 11, the actuator location can be calculated based on the norms of $\mathbf{K} > 19.00$ by NFCG, and the sensor location can be obtained from the norms of $\mathbf{K_e} > 2.60$ by NKFEG. The results with control inputs using MFC are shown in Figs. 12a–12d. The ratio of

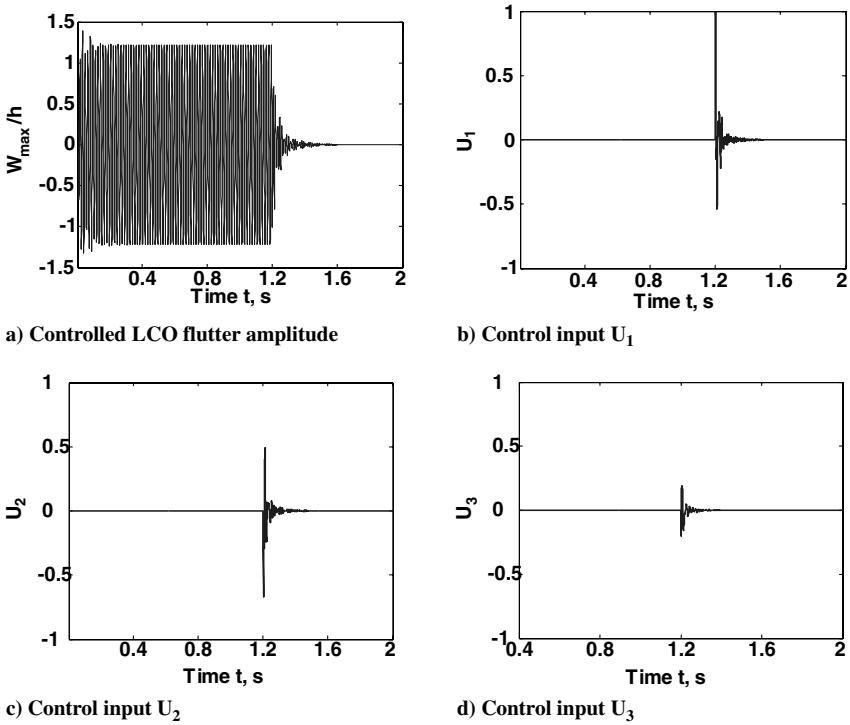

a) Controlled LCO flutter amplitude

b) Control input U_1

c) Control input U_2

d) Control input U_3

Fig. 12 Suppression of LCO using MFC for a clamped rectangular [−40/40/ − 40] composite plate at $\lambda = 800$ and $\Lambda = 60$ deg.

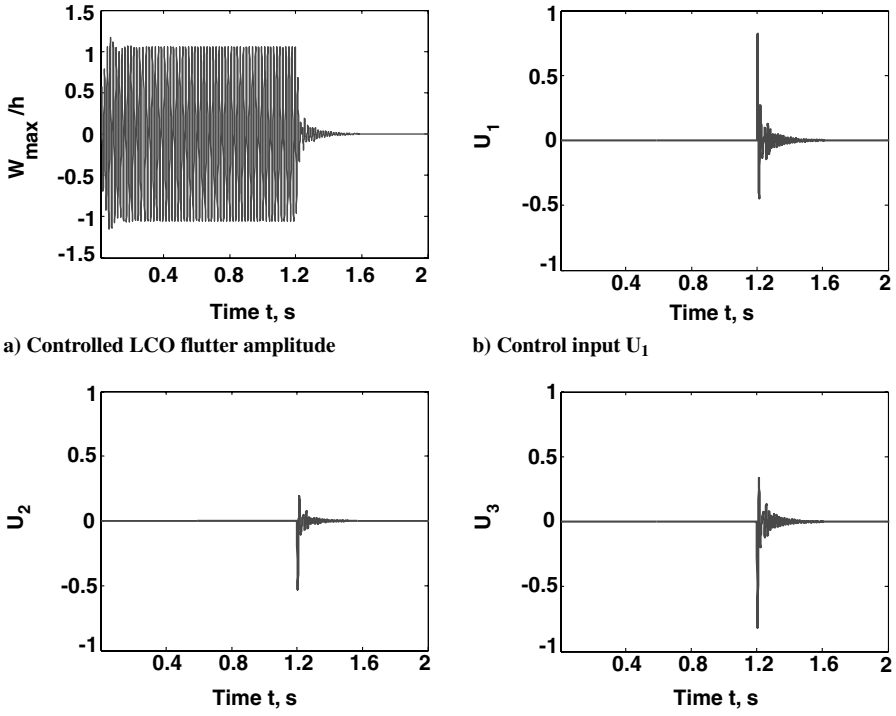

a) Controlled LCO flutter amplitude b) Control input U_1

c) Control input U_2 d) Control input U_3

Fig. 13 Suppression of LCO using MFC for a clamped rectangular [−40/40/ − 40] composite plate at $\lambda = 600$ and $\Lambda = 15$ deg.

$\lambda_{max} = 805$ to $\lambda_{cr} = 480$ is 1.68 using 17.4% actuators of the total panel area. More actuators could be required to improve the control performance. To deal with multiple yaw angles, an another subject flow angle, $\Lambda = 15$ deg, is investigated using the identically constructed controller and optimal location determined at $\Lambda = 60$ deg. In Figs. 13a–13d, the designed regulator can completely suppress the large amplitude of the LCO response, which confirms the pragmatic use of AEM even at any flow angle $0 \text{ deg} \leq \Lambda \leq 90 \text{ deg}$ [5].

V. Conclusions

The finite element nonlinear modal formulation using AE modes is presented in a time domain for suppressing panel flutter at supersonic speeds. Using the AE modal analysis is encouraged because it simplifies the construction of nonlinear active controllers by replacing the system equations of motion with a small size of system matrices. The self-sensing piezoelectric actuators are adopted to suppress large amplitudes of flutter response. The LQR optimal controller with the EKF is developed for controlling LCO motion. The proposed extended Kalman filter considers the nonlinear effect of structural motion and provides optimal estimation of state variables. As for the efficient location of actuators and sensors, the NFCG and NKFEG methods are used by calculating the highest norm of gain values of the LQR controller and the Kalman filter. The control performance of the simply supported isotropic square plate with a zero yaw angle is simulated using PZT5A piezoelectric actuators. The maximum flutter-free dynamic pressure λ_{max} can be increased up to over twice the critical dynamic pressure λ_{cr}. Clamped rectangular composite plates are studied with two different piezoelectric actuators, MFC and PZT5A, with the slightly changed optimal location. The numerical simulation shows that the smaller input power brings better fulfillment of controlling LCO amplitude. By using MFC actuators, the maximum flutter-free dynamic pressure λ_{max} is increased up to over twice the critical dynamic pressure λ_{cr} as well. Additionally, the controller is also designed and applied to the composite panel exposed to yawed flow angle for suppression flutter. The suppressed control response is achieved by using MFC actuators and the ratio $\lambda_{max}/\lambda_{cr}$ is obtained with the high performance. Furthermore, it is worth noting that the presented control approach based on the AEMs is effective to the changed yawed flow angles within 90 deg.

Appendix

Table A1 Material Properties of the Isotropic and Composite Plate, PZT5A and MFC

Materials	Young's modulus, psi	Shear modulus, psi	Poisson's ratio	Density, lb · sec^2/in.^{4}	Charge constant, in./V	V_{max}, V	Thickness, in.
Isotropic	$E = 10.5 \times 10^6$	$G = 3.38 \times 10^6$	$\nu = 0.31$	$\rho = 2.588 \times 10^{-4}$	——	——	——
Graphite epoxy	$E_1 = 22.5 \times 10^6$	$G_{12} = 0.66 \times 10^6$	$\nu_1 = 0.22$	$\rho = 1.458 \times 10^{-4}$	——	——	——
	$E_2 = 1.17 \times 10^6$		$\nu_2 = 0.011$		——	——	——
PZT5A	$E_p = 9.00 \times 10^6$	$G_p = 3.43 \times 10^6$	$\nu = 0.30$	$\rho_p = 7.10 \times 10^{-4}$	$d_{31} = -7.51 \times 10^{-9}$	820	$h_p = 0.009$
MFC	$E_{p1} = 5.29 \times 10^6$	$G_{p12} = 2.12 \times 10^6$	$\nu_{p1} = 0.25$	$\rho_p = 7.07 \times 10^{-4}$	$d_{11} = 2.09 \times 10^{-8}$	2000	$h_p = 0.009$
	$E_{P2} = 1.10 \times 10^6$	$G_{p23} = 1.06 \times 10^6$	$\nu_{p2} = 0.05$		$d_{12} = -8.27 \times 10^{-9}$		

References

[1] Mei, C., Abdel-Motagaly, K., and Chen, R., "Review of Nonlinear Panel Flutter at Supersonic and Hypersonic Speeds," *Applied Mechanics Reviews*, Vol. 52, No. 10, 1999, pp. 321–332.

[2] Zhou, R. C., Xue, D. Y., and Mei, C., "Finite Element Time Domain—Modal Formulation for Nonlinear Flutter of Composite Panels," *AIAA Journal*, Vol. 32, No. 10, 1994, pp. 2044–2052.

[3] Dowell, E. H., "Nonlinear Oscillations of a Fluttering Plate," *AIAA Journal*, Vol. 4, No. 7, 1966, pp. 1267–1275.

[4] Abdel-Motagaly, K., "Finite Element Analysis and Active Control for Nonlinear Flutter of Composite Panels Under Yawed Supersonic Flow," Ph.D. Dissertation, Dept. of Aerospace Engineering, Old Dominion Univ., Norfolk, VA, Dec. 2001.

[5] Guo, X., and Mei, C., "Using Aeroelastic Modes for Nonlinear Panel Flutter at Arbitrary Supersonic Yawed Angle," *AIAA Journal*, Vol. 41, No. 2, 2003, pp. 272–279.

[6] Guo, X., and Mei, C., "Application of Aeroelastic Modes on Nonlinear Supersonic Panel Flutter at Elevated Temperatures," *Computers and Structures*, Vol. 84, Nos. 24–25, 2006, pp. 1619–1628. doi:10.1016/j.compstruc.2006.01.041

[7] Scott, R. C., and Weisshaar, T. A., "Panel Flutter Suppression Using Adaptive Material Actuators," *Journal of Aircraft*, Vol. 31, No. 1, 1994, pp. 213–222.

[8] Surace, G., Ruotolo, R., and Di Terlizzi, D., "Active Control Laws for Panel Exposed to Supersonic Air Flow," *14th International Modal Analysis Conference*, Society for Experimental Mechanics, Inc., Bethel, CT, 1996, pp. 285–291.

[9] Frampton, K. D., Clark, R. L., and Dowell, E. H., "Active Control of Panel Flutter with Piezoelectric Transducers," *Journal of Aircraft*, Vol. 33, No. 4, 1996, pp. 768–774.

[10] Zhou, R. C., Lai, Z., Xue, D. Y., Huang, J. K., and Mei, C., "Suppression of Nonlinear Panel Flutter with Piezoelectric Actuators Using Finite Element Methods," *AIAA Journal*, Vol. 33, No. 6, 1995, pp. 1098–1105.

[11] Doengi, F., Dinkler, D., and Kroeplin, B., "Active Panel Flutter Suppression Using Self-Sensing Piezoactuators," *AIAA Journal*, Vol. 34, No. 6, 1996, pp. 1224–1230.

[12] Abdel-Motagaly, K., Guo, X., Duan, B., and Mei, C., "Active Control of Nonlinear Panel Flutter Under Yawed Supersonic Flow," *AIAA Journal*, Vol. 43, No. 3, 2005, pp. 671–680.

[13] Moon, S.-H., and Kim, S.-J., "Suppression of Nonlinear Composite Panel Flutter with Active/Passive Hybrid Piezoelectric Networks Using Finite Element Methods," *Computers and Structures*, Vol. 59, No. 4, 2003, pp. 525–533. doi:10.1016/S0263-8223(02)00234-9

[14] Moon, S.-H., Chwa, D., and Kim, S. J., "Feedback Linearization Control for Panel Flutter Suppression with Piezoelectric Actuators," *AIAA Journal*, Vol. 43, No. 9, 2005, pp. 2069–2073.

[15] Guo, X., Lee, Y., Mei, C., "Supersonic Nonlinear Panel Flutter Suppression Using Shape Memory Alloys," *Journal of Aircraft*, Vol. 44, No. 4, 2007, pp. 1139–1149. doi:10.2514/1.16080

[16] "IEEE Standard on Piezoelectricity," *ANSI/IEEE Standard 176*, Institute of Electrical and Electronics Engineers, New York, 1978.

[17] Anderson, E. H., and Hagood, N. W., "Simultaneous Piezoelectric Sensing/Actuation: Analysis and Application to Controlled Structures," *Journal of Sound and Vibration*, Vol. 174, No. 5, 1994, pp. 617–639. doi:10.1006/jsvi.1994.1298

[18] Azzouz, M. S., Mei, C., Bevan, J. S., and Ro, J. J., "Finite Element Modeling of MFC/AFC Actuators and Performance of MFC," *Journal of Intelligent Material Systems and Structures*, Vol. 12, No. 9, 2001, pp. 601–612. doi:10.1177/10453890122145384

[19] Bogner, F. K., Fox, R. L., and Schmit, L. A., "The Generation of Inter-Element Compatible Stiffness and Mass Matrices by the Use of Interpolation Formulas," Air Force Flight Dynamics Laboratory TR-66-80, Wright–Patterson Air Force Base, OH, 1966, pp. 396–443.

[20] Meirovitch, L., *Fundamentals of Vibrations*, McGraw–Hill, New York, 2001, p. 346.

[21] Grewal, M. S., and Andrews, A. P., *Kalman Filtering: Theory and Practice Using MATLAB*, Wiley, New York, 2001, pp. 175–184, Chap. 5.

A. Palazotto
Associate Editor